Carbon Vacancy Assisted Contact Resistance Engineering in Graphene FETs

Jeevesh Kumar, *Member, IEEE*, Adil Meersha, Harsha B. Variar, Abhishek Mishra, and Mayank Shrivastava, *Senior Member, IEEE*

***Abstract*— Despite various remarkable properties, the state of the arts of graphene devices are still not up to the mark due to their high contact resistance. The contact resistance milestone has not been achieved yet, probably due to ambiguity in understanding graphene–metal contact properties. In this work, we did a systematic investigation of palladium–graphene contact properties using a density functional theory (DFT) and various process-based experimental approaches. Our study reveals significant interaction of palladium (Pd) with graphene. Their orbitals overlap leads to potential barrier lowering at the interface, which can be reduced further by bringing graphene closer to the bulk Pd using carbon vacancy engineering at the contacts. Thus, the carbon vacancy-assisted barrier modulation reduces contact resistance by increasing carrier transmission probabilities at the interface. The theoretical findings have been emulated experimentally by carbon vacancy engineering at the graphene field-effect transistors (FETs). Different contact-engineered graphene devices with Pd contacts show significant contact resistance reduction, measuring as low as $\sim$78 $\Omega \cdot \mu$m at room temperature. The contact resistance shows a "V" shape curve as a function of defect density. Also, the optimum contact resistance achieved is significantly lower than their pristine counterpart, as predicted by the theoretical estimates. Due to contact engineering, I_{ON} improves by $\sim$6$\times$, transconductance by $\sim$8$\times$, and device mobilities by $\sim$6$\times$ in the device FETs. These investigations and understanding can help to boost the performance of graphene FETs, especially for high-frequency RF applications.**

***Index Terms*— Contact resistance, density functional theory (DFT), graphene, metal, QuantumATK, vacancy.**

I. Introduction

THE metal–graphene contact resistance plays a crucial role in the RF applications of graphene [1]–[7]. There have been several attempts in the past to reduce its value and achieve the contact resistance comparable to the bulk technologies [8]–[19]. Some of these techniques were successful in improving the contact resistance significantly. However, most of the processes developed for improving the metal–graphene contact have an adverse impact on channel mobilities. Additional process steps involving impractical complexities and significant device-to-device variations have also been reported. An in-depth understanding of the metal–graphene interface and the carrier transport across the interface can help in designing efficient contact engineering techniques for graphene field-effect transistors (FETs).

The high contact resistance across metal–graphene interface is mainly due to existing van der Waal's (vdW) gap-based tunnel barriers between graphene and most of the metals, and low carrier density near the Dirac cone [12]. A charge transfer-based model has earlier been used to explore the interaction of various metals with graphene [20]–[27]. However, further understanding of the potential barrier and its modulation at the interface can devise the technique for further reduction in contact resistance. Xia *et al.* [7] predicted a lower limit of contact resistance for the Pd–graphene interface based on Landauer's model, which was also close to the value reported experimentally. The limitation, however, can be broken further by enhancing the interaction between Pd and graphene orbitals by using suitable contact engineering techniques [15], [17]. Ji *et al.* [28] studied the chemisorption and physisorption nature of different metals on graphene. Based on the Fermi-level position, they predicted the absence of a tunnel barrier at the Pd–graphene interface. However, the Fermi-level position can also be tuned with voltage bias during device operation, which needs to be explored.

Anzi *et al.* [17] demonstrated the lowest contact resistance for gold (Au) contact by creating carbon vacancies at the interface, henceforth referred to as vacancy engineering. For further comprehensive understanding, it is imperative to explore the effects of various defect creation processes, size, and density

Manuscript received January 11, 2022; accepted February 2, 2022. Date of publication February 28, 2022; date of current version March 28, 2022. This work was supported in part by the Nanoelectronics Network for Research and Application (NNetRA) Program of the Ministry of Electronics and Information Technology (MeitY), the Department of Science and Technology (DST), and the Ministry of Human Resource Development (MHRD), Government of India; in part by the Defence Research and Development Organisation (DRDO); and in part by the Council of Scientific and Industrial Research (CSIR). The review of this article was arranged by Editor A. M. P. Anantram. *(Jeevesh Kumar and Adil Meersha contributed equally to this work.) (Corresponding author: Jeevesh Kumar.)*

Jeevesh Kumar, Harsha B. Variar, and Mayank Shrivastava are with the Department of Electronic Systems Engineering, Indian Institute of Science, Bengaluru 560012, India (e-mail: jeevesh@iisc.ac.in; mayank@iisc.ac.in).

Adil Meersha was with the Department of Electronic Systems Engineering, Indian Institute of Science, Bengaluru 560012, India. He is now with the Cambridge Graphene Centre, University of Cambridge, Cambridge CB3 0FA, U.K. (e-mail: adil@alum.iisc.ac.in).

Abhishek Mishra was with the Department of Electronic Systems Engineering, Indian Institute of Science, Bengaluru 560012, India, and also with the Center for Nanoscience and Engineering, Indian Institute of Science, Bengaluru 560012, India. He is now with the Centre for Device Thermography and Reliability, H. H. Wills Physics Laboratory, University of Bristol, Bristol BS8 1TL, U.K. (e-mail: mishra@alum.iisc.ac.in).

Color versions of one or more figures in this article are available at https://doi.org/10.1109/TED.2022.3151033.

Digital Object Identifier 10.1109/TED.2022.3151033

of defects on contact resistance. Ghatge and Shrivastava [29] used computational methods to explore the mechanism behind reduction in contact resistance due to carbon vacancies. However, various important aspects, including potential barrier modulation, charge transfer direction at metal–graphene interface, and modulation of work function under metal, are yet to be explored. Thus, a detailed computational investigation is required to understand the mechanism behind vacancy engineering at the metal–graphene interface to estimate the contact resistance. Besides, there is also a need for experimental investigation to explore various processing steps to create carbon vacancy in graphene and the role of defect density over contact resistance and other FETs parameters.

In this work, we provide a detailed computational study of carbon vacancy engineering-assisted reduction in contact resistance and its experimental validation. This article is organized as follows. Section II provides the computational and experimental details. Section III discusses palladium–graphene quantum chemistry, and Section IV is about barrier modulation at the Pd–graphene interface. Subsequently, vacancy-assisted orbitals overlap, vacancy-assisted barrier lowering and contact resistance estimation, and interface charge transfer mechanism are discussed in Sections V–VII, respectively. Finally, the experimental validation of reduction in contact resistance through vacancy engineering is provided in Section VIII. The experimental validation is based on different techniques to remove carbon atoms from graphene, namely, comb patterning, Ar/O_2 reactive ion etching (RIE), Ar/O_2 ashing inside a metal evaporator, and controlled vacancy creation through e-beam. Although the metal palladium has been used for various computational studies and experiments, the discussion can be extended to other metals as well. The selection of palladium is due to its chemisorption nature over graphene and its broad acceptance as a contact metal for graphene devices [21].

II. Computational and Experimental Details

The density functional theory (DFT)-based [30] quantum computational method, supported by QuantumATK package [31], [32], was used in all the computational works.

A. Computed Modules and Parameters

Two different configurations of palladium were considered in the simulations—atomic and bulk palladium. To study the interaction of graphene with atomic palladium, four palladium atoms were kept over a 7×7 supercell of pristine graphene [see Fig. 1(a)] and graphene with a single carbon vacancy (vac. graphene) [see Fig. 4(a)]. These structures were optimized for minimum energy before computing other parameters for analysis. Similarly, for simulating interface with bulk palladium, Pd (111)–graphene interfaces were created for pristine [see Fig. 2(a)] as well as vac. graphene [see Fig. 6(a)]. Eight Pd layers were considered to emulate the bulk effect of palladium. Interfacial strain developed at the interface was distributed equally among Pd and graphene layers. The vacuum space of ~30 Å was added along the z-axis (perpendicular to graphene plane) in the supercells to avoid interactions from the corresponding mirror modules along the z-axis due to periodic boundary conditions. Energy optimization of all the supercells was done with 0.01-eV/Å force and 0.001-eV/Å^3 energy cutoffs. The Perdew–Burke–Ernzerhof (PBE) form of generalized gradient approximation (GGA) [33] functional was used in DFT computation with $10 \times 10 \times 1$ k point sampling for all the modules. Grimme-D2 Van der Walls (vdW) correction [34] was considered in the calculations to capture long-range vdW interactions.

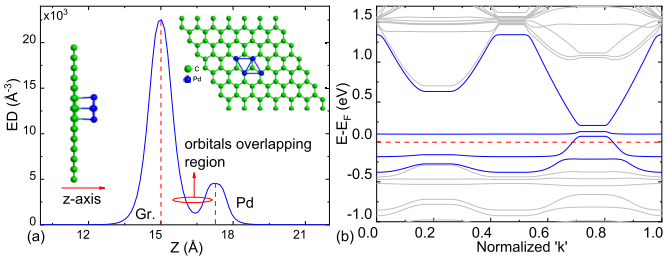

Fig. 1. (a) Optimized 7×7 supercell of graphene with four palladium atoms (inset) and their electron density (ED) profile along the interacting line (out of the plane of graphene). (b) Band structure of the Pd–graphene system. The band structures is plotted with normalized "κ," which is along $G \rightarrow M \rightarrow L \rightarrow A \rightarrow G \rightarrow K \rightarrow H \rightarrow A$. Positions of *G, M, L, A, G, K, H*, and *A* points on the *k*-axis are 0, 0.172, 0.258, 0.430, 0.516, 0.715, 0.801, and 1.0, respectively. Fermi energy is at zero energy level in all the band structure plots.

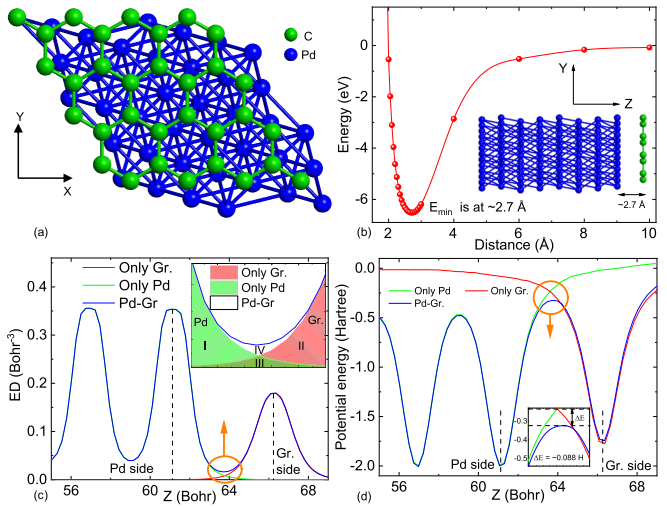

Fig. 2. (a) Top view of Pd–graphene interface. (b) Bond energy versus interfacial distance curve of the system. (c) ED comparison of the system with only graphene and Pd at the same positions. ED of only graphene and Pd overlaps at the interface (inset, III), which increases the ED of the system (inset, IV) at the corresponding regime. (d) System's potential profile comparison with only graphene and Pd at the same positions. Barrier potential at the interface lowers by 0.088 Hartree (inset) due to orbitals overlap of Pd and graphene. Z line is the length of the unit cell perpendicular to the graphene plane (along the approaching line).

B. Device Processing and Characterization

Graphene grown on copper was transferred to SiO_2 (300 nm) on Si using the PMMA-based transfer process [35]. Various contact engineering steps were performed on graphene to create carbon vacancies at the metal–graphene interface just before the metal deposition. Evaporated Pd/Au 30/30 nm was used as the contact metal for all the devices. E-beam lithography was used for the device fabrication process with PMMA as the resist. All the electrical measurements were

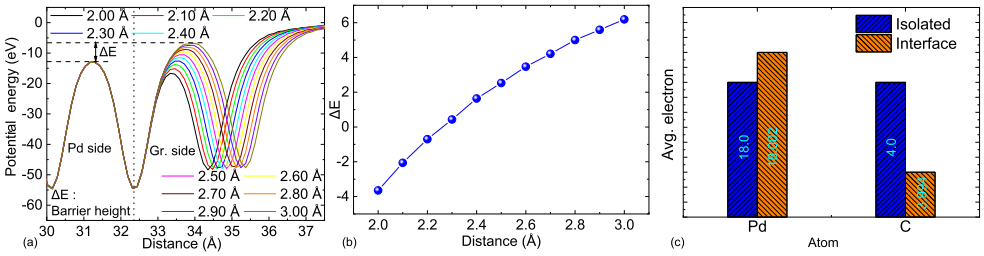

Fig. 3. (a) Potential energy profile of Pd–graphene interfaces with multiple interface distances. (b) Energy barrier height at different Pd–graphene interfacial distances. (c) Mulliken charge (electron) sharing of Pd and carbon in isolated as well as bonded condition (bond distance is 2.7 Å). Energy barrier height at the interface is decreased with a reduction in interfacial distances. Charge sharing of Pd and C are increased and decreased, respectively. Thus, the valence charge of carbon atoms is drifted toward Pd due to bonding at the interface.

performed using Keithley 4200, and Raman measurements were performed using Horiba Labram HR with a 532-nm laser source at room temperature.

III. Palladium–Graphene Quantum Chemistry

For a systematic understanding of Pd–graphene interface, we begin with an investigation of the interaction of a few Pd atoms with graphene and explore their chemistry.

Four Pd atoms were placed over a 7 × 7 supercell of pristine graphene and optimized using DFT to achieve their minimum energy [see Fig. 1(a)]. The minimum distance of the Pd atom from the graphene surface is ∼2.14 Å. The interacting system has significant electron density (ED) in its bonding regime [see Fig. 1(a)], reflecting strong orbitals overlap between graphene and Pd atoms. Their interaction rehybridizes the local wave function, which perturbs the band structure of graphene [see Fig. 1(b)]. Moreover, the Dirac cone of graphene disappears, and its Fermi level moves inside the valence band. Thus, when bulk Pd metal approaches graphene during contact formations, their work functions can be modulated by virtue of their orbitals overlaps, as observed experimentally by Song *et al.* [11]. The work function modulation along with local orbitals interactions can reshape the local potential profile, thereby affecting the carrier transport barrier parameters at the interface. Thus, it is worth highlighting that the contact behavior of Pd–graphene interface cannot be adequately predicted by the work function alignment only.

IV. Barrier Modulations at Graphene Contact

After investigating the strong affinity of atomic Pd with graphene, a Pd–graphene bulk interface structure [see Fig. 2(a)] was investigated for further understanding of its contact properties. The system has minimum energy at ∼2.7 Å [see Fig. 2(b)], which is the optimum interfacial distance of bulk Pd from pristine graphene. In such proximity, their orbitals can overlap and modulate the potential profile at the interface [24]. ED of Pd and graphene [see Fig. 2(c)] clearly says that their orbitals overlap along the approaching line (z-axis). The Pd–graphene system has higher ED in the overlapping regions than their individual electron densities, reflecting that graphene has strong interaction with Pd in such closer proximity. The potential profile of the Pd–graphene system is modulated [see Fig. 2(d)] due to the strong interactions. The energy barrier of the system at the interface is ∼0.088 Hartree (2.39 eV) lower than the estimated barrier. This confirms that barrier height for the carriers, and hence transport across the Pd–graphene interface, cannot be predicted using their work function difference only, as it is modulated by the interactions between Pd and graphene.

Modulation of the potential at the interface can be visualized by comparing potential profiles at the interface with the approaching distance of graphene from Pd [see Fig. 3(a) and (b)]. The reduction in distance between graphene and Pd modulates the potential profile near the interface and causes a decrease in the barrier height [see Fig. 3(a) and (b)]. Although the barrier height still exists at an optimum interfacial distance (2.7 Å), it is argued that a further reduction in barrier height is possible by suitable contact engineering approaches.

Charge sharing calculations at the optimum interfacial distance reveal that Pd/carbon has more/less charge sharing than the corresponding isolated conditions [see Fig. 3(c)]. Thus, electron drifts from graphene to Pd during the bonding process of their orbitals.

V. Vacancy-Assisted Orbital Overlaps

In this section, we investigate the effect of carbon vacancies on the potential barrier between graphene and palladium. It is argued that a carbon vacancy in graphene (vacancy engineering) at the interface would strengthen the Pd–graphene bonds due to enhanced interactions of Pd with unsaturated orbitals of carbon atoms near the vacant site. To verify the vacancy-assisted enhanced interaction of palladium and graphene, we have investigated the interactions of four Pd atoms with graphene, which has one carbon vacancy (vac. graphene) at the center of the supercell [see Fig. 4(a)]. All four Pd atoms come over the top of the carbon atoms after energy optimization, among which three carbon atoms (see Fig. 4(a): 1, 2, and 3) are adjacent to vacancy and have unbonded orbitals. The minimum distance of Pd from the carbon atom is ∼1.97 Å, which reflects that Pd has a stronger interaction with the vac. graphene than pristine one (∼2.14 Å). A comparison of Mullikan charge in vacancy-engineered interface with the pristine interface [see Fig. 4(b)] shows that carbon shares more charge than palladium in case of the engineered interface, indicating a drift in charge from palladium to carbon.

Carbon vacancy-assisted orbitals overlap enhancement can be explored further by analyzing their atomic and orbitals

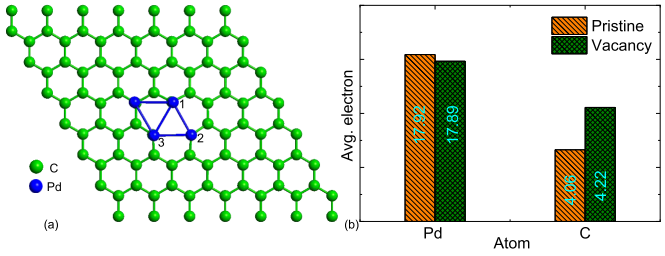

Fig. 4. (a) Top view of a 7 × 7 supercell of graphene with four palladium atoms which has one carbon vacancy at the center. (b) Mulliken charge (electron) sharing comparison of Pd and overlapping carbon atoms (1, 2, and 3) in, isolated state, Pd over pristine graphene [see Fig. 1(a)] and Pd over vac. graphene.

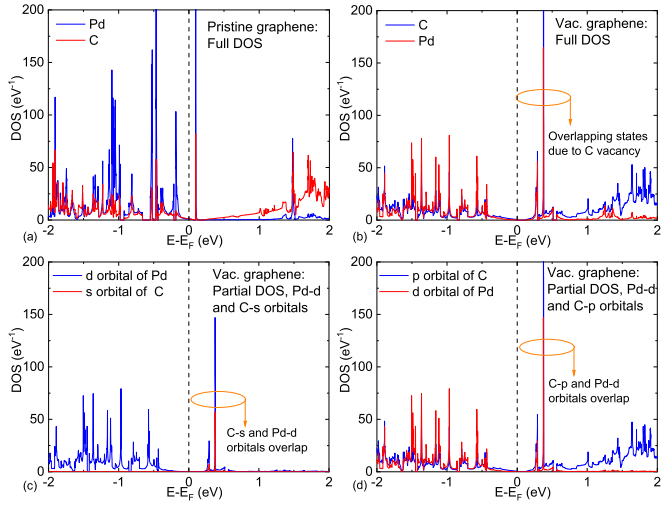

Fig. 5. Overlapping DOSs of Pd over pristine as well as vac. graphene: (a) Pd and C total DOS of pristine graphene, (b) Pd and C total DOS of vac. graphene, (c) s-orbital of C and d-orbital of Pd DOS of vac. graphene, and (d) p-orbital of C and d-orbital of Pd DOS of vac. graphene.

density of states (DOSs) to understand different orbitals' contributions in the bonding (see Fig. 5). Carbon and Pd have more overlapping DOS near the Fermi level in vac. graphene than pristine graphene [see Fig. 5(a) and (b)]. Thus, their orbitals overlap enhances after creating carbon vacancy in pristine graphene. The corresponding orbitals DOS comparison [see Fig. 5(c) and (d)] reflects that the overlapping DOS near Fermi energy has the major contribution of p-orbital of carbon and d-orbital of Pd. Therefore, bonding enhancement is due to unbonded orbitals of unsaturated carbon atoms at the vacant site.

VI. Vacancy-Assisted Barrier Lowering

In the previous section, we discussed the role of carbon vacancies in enhancing the interaction between orbitals of carbon and palladium, thereby decreasing the barrier width. An equally important parameter for transport across the interface is the barrier height. In this section, we discuss the effect of carbon vacancies on barrier height between palladium and carbon. We consider a Pd–graphene interface with a carbon vacancy at the center of the supercell [see Fig. 6(a)]. The system achieves its minimum energy when graphene is ∼2.5 Å away from Pd [see Fig. 6(b)], which is ∼0.2 Å shorter

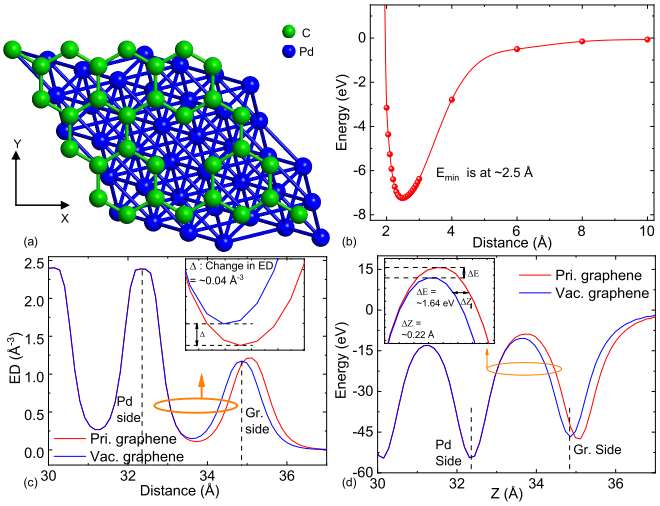

Fig. 6. (a) Top view of Pd–graphene interface having a carbon vacancy. (b) Bond energy versus interfacial distance curve of the system. (c) ED comparison of the system with the corresponding pristine counterpart. (d) Potential profile comparison of the systems.

than its pristine counterpart (see Fig. 2). A comparison of ED in the vac. graphene–Pd system with the corresponding pristine graphene–Pd system [see Fig. 6(c)] clearly shows that the vac. graphene–Pd system has higher ED in the interface regime. Minimum ED in the bonding regime for vac. graphene is higher than its pristine counterpart, which says that the system has higher orbital overlaps due to carbon vacancy. Due to strong orbital overlaps, the system releases ∼7.24-eV energy, which is ∼0.72 eV higher than the corresponding pristine structure (6.52 eV). The interaction enhancement due to carbon vacancy (vac. engineering) not only reduces barrier height but also the barrier width at the interface [see Fig. 6(d)]. Barrier height and barrier width in the vac. graphene system are ∼1.64 eV lower and ∼0.22 Å shorter than those in the pristine graphene system, respectively. The reduction in barrier height and width would enhance carrier transmission probability through the interface. Thus, the process can reduce the contact resistance of the corresponding devices.

In order to quantify the reduction in contact resistance, we model the Pd–graphene interface as a step potential barrier, with barrier height V and width a.

The transmission probability of an electron, having energy E, through step potential barrier is given by, $T(E) = (16E/V)(1-(E/V))\exp(-2ka)$, where $k = ((2m(V-E))/\hbar^2)^{1/2}$.

The expression highlights that carrier transmission probability is an exponential function of barrier height and width. Using the barrier heights [ΔE in Fig. 3(a)] of ∼4.17 and ∼2.57 eV for pristine and vac. interfaces, respectively, and average barrier widths of ∼0.87 and ∼0.65 Å for pristine and vac. interfaces (see Fig. 6(d), inset), respectively, we find that the transmission probability across vac. interface is 1.5× more than the pristine interface. Moreover, the inverse dependence of contact resistance on transmission probability ($(1/R_C) \propto \int T(E)$) suggests a ∼1.5× reduction in contact resistance due to vacancy engineering.

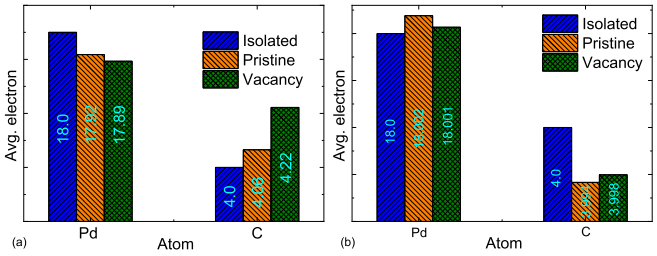

Fig. 7. Mulliken charge (electron) comparison of carbon and Pd: (a) atomic Pd–graphene interface and (b) bulk Pd–graphene interface. For Pd, the charge is averaged over all the Pd atoms. For carbon, the charge is averaged over neighbor carbon atoms at the vacant site.

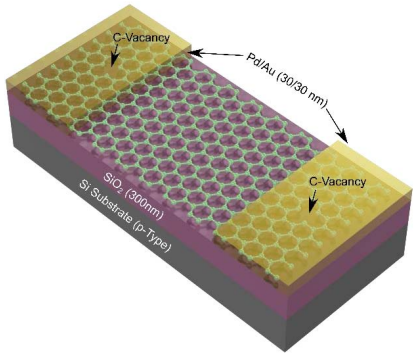

Fig. 8. Proposed carbon vacancy-engineered back-gated graphene FET. Carbon vacancies were created below metal contacts using different process engineering.

It should be noted that an approximate model has been used here to quantify the enhancement in the transmission probability. A comprehensive model would include the change in carrier density at the interface, accurate model of barrier profile, sheet resistivity below metal, and temperature. Consequently, the vacancy engineering would result in $>1.5\times$ reduction in contact resistance [36]. As discussed in the later section, the vacancy-engineered Pd–graphene devices show $>1.5\times$ reduction in contact resistance than the corresponding pristine devices.

VII. Interface Charge Transfer Mechanism

A closer look at charge (electron) sharing using the Mulliken charge population at the Pd–graphene interacting systems reveals charge sharing strategies of the atoms during interactions. Pd and C have 18 and 4 valence electrons, respectively. For atomic interactions (see Figs. 1 and 4), the average electron around Pd/C atoms is reduced/increased for pristine and vac. graphene systems, respectively [see Fig. 7(a)]. For bulk interactions [see Figs. 2(a) and 6(a)], the charge around Pd/C is increased/reduced for the pristine interface, which, however, is reduced/increased again when carbon vacancy is created at the interface [see Fig. 7(b)]. Thus, charge flow direction depends on whether Pd is atomic or bulk. It is also a signature of interaction type, whether physical or chemical. For atomic Pd, charge drifts from Pd to carbon due to their electronegativity difference (carbon is more electronegative than Pd). Carbon vacancy brings Pd closer, which drifts the bonded charge further from Pd to carbon. On the other hand, for bulk Pd (multi Pd layers), the Pd layer stays away ($\sim$2.7 Å) from pristine graphene where vdW interaction dominates. In such a condition, the charge drifts from graphene to Pd due to Pd's higher work function ($\sim$5.2 eV) than graphene ($\sim$4.7 eV). Carbon vacancy at the interface enhances chemical interaction, which drifts bonded again to carbon (high electronegativity side) despite its lower work function than Pd.

The charge transfer due to bonding may not directly affect contact resistance reduction. However, the mechanism helps in understanding bonding strength at the interface and distinguishing the interactive nature of graphene with atomic and bulk palladium.

Reducing energy barrier height and width at the interface by approaching metal to graphene gives a knob to engineer the contact resistance further. Contact resistance can be reduced further by further decreasing the interfacial distance of graphene and Pd. Putting vertical stress at the interface, enhancing bonding by putting intermediate chemically reactive elements, or changing carbon vacancy density at the interface are some of the engineering methods that can further improve the Pd–graphene contact resistance.

VIII. Experimental Validation of Vacancy-Assisted Contact Engineering

The DFT-based investigations revealed that carbon vacancies at the graphene–Pd interface can reduce the corresponding contact resistance significantly. In this section, we discuss various controlled techniques to create vacancies at graphene–metal interface. Highly controlled dry etching processes are required to knock off a few carbon atoms selectively before metal depositions over graphene (see Fig. 8). We discuss four different techniques, as discussed later, to create controlled carbon vacancies in graphene. The contact resistance of vacancy-engineered graphene FETs is compared with the FETs having pristine (without vacancies) metal–graphene interface. A minimum of 40 TLM devices (see Fig. 9) were fabricated in each of these processes. The statistic of the variation of contact resistance for a given process (see Fig. 12) and the variation of contact resistance within the best optimized process for each engineering technique (see Fig. 13) are also discussed later. Four different vacancy engineering techniques are used to create carbon vacancy at metal–graphene interface. These techniques are discussed as follows.

A. Comb Patterning

Graphene at the interface was patterned to have larger effective edge contacting regions to form comb-like structures. This ensures that larger edges of graphene, naturally carbon vacant, contact the metal on top for a given contact area. This patterned edge acts like the defect sites at the interface. The comb patterning was done along with the channel patterning in order to avoid additional patterning. The edge perimeter (P_E) was estimated, as shown in Fig. 9. In this process, the graphene channel remained unaffected, and only the edges of graphene, in contact with the metal, were utilized for contact engineering.

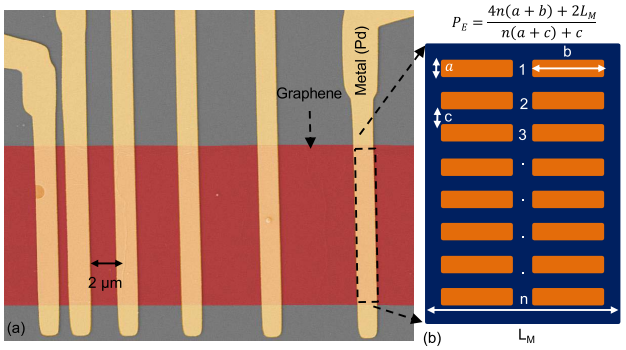

Fig. 9. (a) False color SEM if the TLM fingers fabricated. (b) Comb architecture below the metal figure and the corresponding estimation of the edge perimeter (P_E).

B. Ar/O_2 Reactive Ion Etching

Graphene at the interface was defected using O_2/Ar plasma using an ICP-RIE system (Oxford PlasmaLab System 100). A low plasma density was maintained by keeping a gas flow rate of O_2/Ar at 10 sccm and an RF power of 10 W. The plasma exposure was done immediately after contact metal lithography and development. After RIE, the sample was immediately loaded inside the metal evaporation system to avoid significant exposure to oxygen and moisture. The RIE duration was varied for different dies/substrates, and the corresponding contact resistance was measured.

C. Ar/O_2 Ashing Inside a Metal Evaporator

In this case, the metal–graphene interface was engineered using an in-built ion Asher inside a metal evaporator (TECPORT). The sample was patterned with E-beam lithography like in case B for contact metal deposition and was developed before loading into the evaporator system. A gas flow rate of 1 sccm O_2/Ar was maintained for a duration of 1 min at 20 V. The defect creation and metal deposition take place with the same vacuum and hence prevents interaction of the defect sites, after formation, with oxygen or moisture before the metal deposition. There is no additional lithography required for this case as well.

D. E-Beam-Based Defect Creation

Graphene TLM structures were loaded back into an electron beam lithography system (Raith Eline) after contact metal lithography and development. The graphene at the interface was defected using the electron beam at 30-kV EHT, 20-μm aperture, 30-nm step size, and varying doses ($e-1$). This technique provides highly localized defects with controllable defect density. The same defect creation process was also implemented in combination with the best case of the comb-patterned graphene at the metal–graphene interface ($e-2$).

Vacancy engineering using all the methods discussed above was implemented over different graphene samples before metal deposition. G/D peaks ratios in Raman spectra of graphene, exposed under oxygen plasma with different exposure times, clearly reflect that defect density

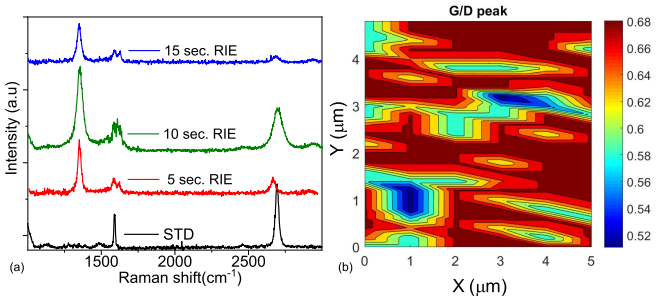

Fig. 10. (a) Raman spectra extracted for as-grown graphene monolayer (STD) as well as graphene exposed to O_2 plasma with different exposure times. (b) G/D peak extracted across 5 μm $\times$ 5 μm of graphene area exposed to O_2 plasma for 10 s.

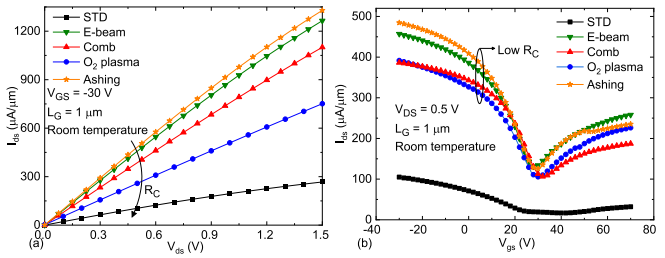

Fig. 11. (a) I_{ds}–V_{ds} and (b) I_{ds}–V_{gs} characteristics of selected contact-engineered devices compared to the standard device without any contact engineering.

increases in graphene with an increase in plasma exposure time (see Fig. 10). Drain-to-source current (I_{ds}) in all the contact-engineered devices is higher than the pristine graphene device, as shown in Fig. 11. All the devices have the same channel parameters; thus, it is worth saying that increment in I_{ds} is due to reduction in the contact resistance.

We achieved a significant reduction in the metal–graphene contact resistance in all the defect creation techniques. The contact resistance versus defect density (proportional to the duration of defect creation) shows a "V" curve in all the cases, signifying an optimum defect density for achieving the lowest possible contact resistance (see Fig. 12). Contact resistance reduces with the increase in defect density due to more orbitals overlaps and reaches the lowest value possible with the given process before it starts to increase due to the current crowding at the metal–graphene interface. Furthermore, we have compared contact resistances of all the engineered devices processed at the corresponding optimized defect density (see Fig. 13). The resistances with O_2 plasma exposure and e-beam show the least values, which are 78 and 84 $\Omega \cdot \mu$m, respectively, at room temperature.

The increase in defect density leads to improved contact resistance and consequently to superior transistor properties. At shorter channel lengths, channel mobility is limited by contact resistance, which seriously degrades the transistor performance and the intrinsic capabilities of graphene. Extracted transconductances and mobilities [37] of the pristine and contact-engineered devices (see Fig. 14) depict that the overall field-effect device mobility significantly improves when contact resistance is lowered. Without contact engineering, ON current was found to be limited, which does not significantly

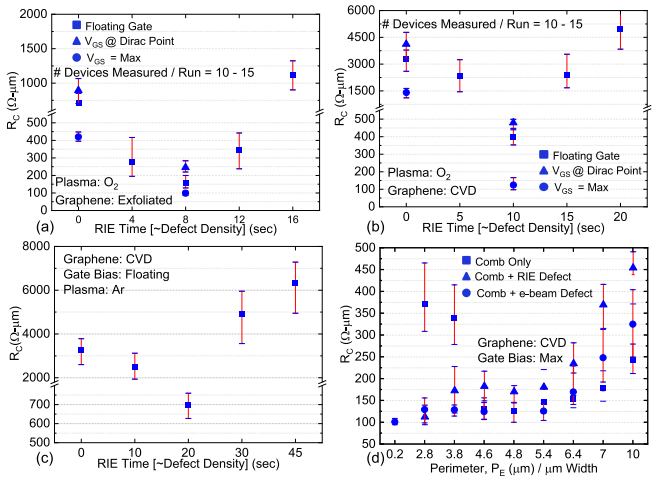

Fig. 12. Contact resistance (R_C) versus the defect density plots with O_2 RIE-based (Case B) contact engineering for (a) exfoliated and (b) CVD. (c) Impact of Ar RIE-based (Case B) contact engineering. (d) R_C extracted using fabricated TLM test structures as a function of edge perimeter of lithographically patterned edges (Case A) along with electron-beam exposure (Case D). A perimeter of 0.2 indicates the TLM device with no comb patterning (standard device).

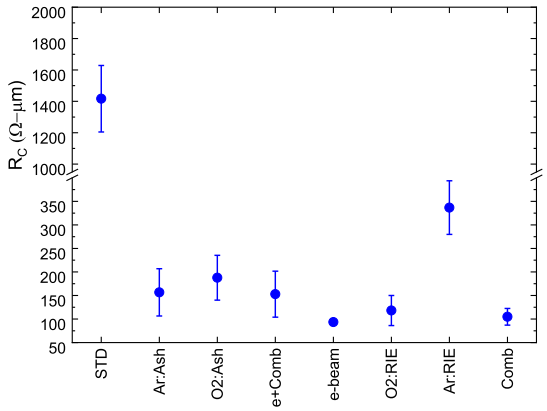

Fig. 13. Contact resistance extracted using fabricated TLM test structures as a function of the contact engineering process at the corresponding optimized defect density.

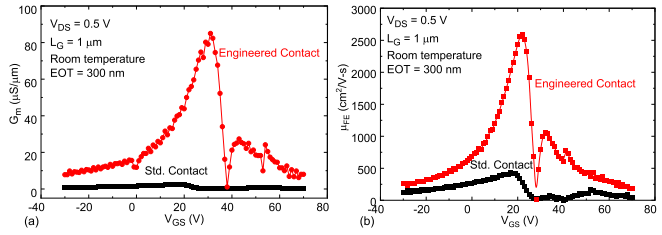

Fig. 14. (a) Transconductance (G_m) and (b) channel field-effect mobility (μ_{FE}) of pristine and the best contact-engineered devices (E-beam based defect creation) as a function of applied gate bias (V_{gs}).

improve with the channel length. Attributed to the superior device performance due to engineered contacts, I_{ON} improves by ~6×, transconductance by ~8×, and device mobilities by ~6×. Clearly, the carbon vacancy-assisted contact engineering by atomic orbital overlap enhancement has allowed graphene FETs to move closer to their intrinsic limits.

IX. Conclusion

In summary, theoretical and experimental approaches have explored the systematic investigation of graphene–Pd contact properties. We have observed that Pd has significant interaction with graphene in atomic and bulk form. Once bulk Pd approaches graphene, it modulates and reduces the potential barrier height at the interface, reducing contact resistance with the reduction in interfacial distance. Carbon vacancy in graphene enhances orbitals' overlap at the interface, which causes an increase in ED and reduction and thinning of the potential barriers. The modulation in potential barrier due to vacancy enhances carrier transmission probability significantly across the interface. Therefore, carbon vacancy reduces contact resistance at the Pd–graphene interface mainly due to tunnel barrier modulation, which improves their orbitals overlap. Besides, charge transfer between graphene and Pd is not unidirectional. Although, for long-range interaction, charge transfers from graphene to Pd, however, it drifts from Pd to graphene during short-range interactions. Experimentally, introducing these defects at the metal graphene, utilizing various contact engineering techniques, consistently reduces contact resistance to very low values. The contact resistance reduces with defect density and reaches the lowest values before increasing due to current crowding and morphological changes on graphene at high defect densities. We achieved the contact resistance as low as ~78 and ~84 $\Omega \cdot \mu$m using O_2 plasma and e-beam-based engineering approaches. The optimum defect density gives superior transistor properties and brings graphene device performance close to its intrinsic nature.

References

[1] K. S. Novoselov *et al.*, "Electric field effect in atomically thin carbon films," *Science*, vol. 306, no. 5696, pp. 666–669, 2004.
[2] S. V. Morozov *et al.*, "Giant intrinsic carrier mobilities in graphene and its bilayer," *Phys. Rev. Lett.*, vol. 100, no. 1, Jan. 2008, Art. no. 016602.
[3] C. Lee, X. Wei, J. W. Kysar, and J. Hone, "Measurement of the elastic properties and intrinsic strength of monolayer graphene," *Science*, vol. 321, no. 5887, pp. 385–388, 2008.
[4] Z. Chen *et al.*, "Synergistic effects of plasmonics and electron trapping in graphene short-wave infrared photodetectors with ultrahigh responsivity," *ACS Nano*, vol. 11, no. 1, pp. 430–437, Jan. 2017.
[5] A. A. Balandin *et al.*, "Superior thermal conductivity of single-layer graphene," *Nano Lett.*, vol. 8, no. 3, pp. 902–907, 2008.
[6] H. S. S. R. Matte, K. S. Subrahmanyam, and C. N. R. Rao, "Novel magnetic properties of graphene: Presence of both ferromagnetic and antiferromagnetic features and other aspects," *J. Phys. Chem. C*, vol. 113, no. 23, pp. 9982–9985, 2009.
[7] F. Xia, V. Perebeinos, Y. Lin, Y. Wu, and P. Avouris, "The origins and limits of metal-graphene junction resistance," *Nature Nanotechnol.*, vol. 6, no. 3, pp. 179–184, 2011.
[8] Q. Kong *et al.*, "Achieving low contact resistance by engineering a metal–graphene interface simply with optical lithography," *ACS Appl. Mater. Interfaces*, vol. 9, no. 25, pp. 21573–21578, 2017.
[9] V. Passi *et al.*, "Contact resistance study of 'edge-contacted' metal-graphene interfaces," in *Proc. 46th Eur. Solid-State Device Res. Conf. (ESSDERC)*, Sep. 2016, pp. 236–239.
[10] A. Gahoi, S. Wagner, A. Bablich, S. Kataria, V. Passi, and M. C. Lemme, "Contact resistance study of various metal electrodes with CVD graphene," *Solid-State Electron.*, vol. 125, pp. 234–239, Nov. 2016.
[11] S. M. Song, J. K. Park, O. J. Sul, and B. J. Cho, "Determination of work function of graphene under a metal electrode and its role in contact resistance," *Nano Lett.*, vol. 12, no. 8, pp. 3887–3892, Aug. 2012.
[12] H.-Y. Park *et al.*, "Extremely low contact resistance on graphene through n-type doping and edge contact design," *Adv. Mater.*, vol. 28, no. 5, pp. 864–870, Feb. 2016.

[13] M. G. Hahm *et al.*, "Low interfacial contact resistance of Al-graphene composites via interface engineering," *Nanotechnology*, vol. 26, no. 21, May 2015, Art. no. 215603.
[14] W. S. Leong, H. Gong, and J. T. L. Thong, "Low-contact-resistance graphene devices with nickel-etched-graphene contacts," *ACS Nano*, vol. 8, no. 1, pp. 994–1001, Jan. 2014.
[15] A. Meersha *et al.*, "Record low metal—(CVD) graphene contact resistance using atomic orbital overlap engineering," in *IEDM Tech. Dig.*, Dec. 2016, pp. 5.3.1–5.3.4.
[16] D. Berdebes, T. Low, Y. Sui, J. Appenzeller, and M. S. Lundstrom, "Substrate gating of contact resistance in graphene transistors," *IEEE Trans. Electron Devices*, vol. 58, no. 11, pp. 3925–3932, Nov. 2011.
[17] L. Anzi *et al.*, "Ultra-low contact resistance in graphene devices at the Dirac point," *2D Mater.*, vol. 5, no. 2, Feb. 2018, Art. no. 025014.
[18] V. Passi *et al.*, "Ultralow specific contact resistivity in metal–graphene junctions via contact engineering," *Adv. Mater. Interfaces*, vol. 6, no. 1, Jan. 2019, Art. no. 1801285.
[19] F. Liu, W. T. Navaraj, N. Yogeswaran, D. H. Gregory, and R. Dahiya, "van der Waals contact engineering of graphene field-effect transistors for large-area flexible electronics," *ACS Nano*, vol. 13, no. 3, pp. 3257–3268, 2019.
[20] G. Giovannetti, P. A. Khomyakov, G. Brocks, V. M. Karpan, J. van den Brink, and P. J. Kelly, "Doping graphene with metal contacts," *Phys. Rev. Lett.*, vol. 101, no. 2, Jul. 2008, Art. no. 026803.
[21] K. T. Chan, J. B. Neaton, and M. L. Cohen, "First-principles study of metal adatom adsorption on graphene," *Phys. Rev. B, Condens. Matter*, vol. 77, no. 23, Jun. 2008, Art. no. 235430.
[22] Q. J. Wang and J. G. Che, "Origins of distinctly different behaviors of Pd and Pt contacts on graphene," *Phys. Rev. Lett.*, vol. 103, no. 6, Aug. 2009, Art. no. 066802.
[23] M. Vanin, J. J. Mortensen, A. K. Kelkkanen, J. M. Garcia-Lastra, K. S. Thygesen, and K. W. Jacobsen, "Graphene on metals: A van der Waals density functional study," *Phys. Rev. B, Condens. Matter*, vol. 81, no. 8, Feb. 2010, Art. no. 081408.
[24] C. Gong, G. Lee, B. Shan, E. M. Vogel, R. M. Wallace, and K. Cho, "First-principles study of metal–graphene interfaces," *J. Appl. Phys.*, vol. 108, no. 12, 2010, Art. no. 123711.
[25] B. J. Schultz, C. Jaye, P. S. Lysaght, D. A. Fischer, D. Prendergast, and S. Banerjee, "On chemical bonding and electronic structure of graphene–metal contacts," *Chem. Sci.*, vol. 4, no. 1, pp. 494–502, 2013.
[26] P. Khakbaz *et al.*, "DFT study of graphene doping due to metal contacts," in *Proc. Int. Conf. Simulation Semiconductor Processes Devices (SISPAD)*, Sep. 2019, pp. 1–4.
[27] T. Cusati *et al.*, "Electrical properties of graphene-metal contacts," *Sci. Rep.*, vol. 7, no. 1, pp. 1–11, Dec. 2017.
[28] X. Ji, J. Zhang, Y. Wang, H. Qian, and Z. Yu, "A theoretical model for metal–graphene contact resistance using a DFT-NEGF method," *Phys. Chem. Chem. Phys.*, vol. 15, no. 41, pp. 17883–17886, 2013.
[29] M. Ghatge and M. Shrivastava, "Physical insights on the ambiguous metal–graphene interface and proposal for improved contact resistance," *IEEE Trans. Electron Devices*, vol. 62, no. 12, pp. 4139–4147, Dec. 2015.
[30] W. Kohn and L. J. Sham, "Self-consistent equations including exchange and correlation effects," *Phys. Rev.*, vol. 140, no. 4A, pp. A1133–A1138, Nov. 1965.
[31] J. M. Soler *et al.*, "The SIESTA method for *ab initio* order-*N* materials simulation," *J. Phys., Condens. Matter*, vol. 14, no. 11, p. 2745, 2002.
[32] *QuantumWise ATK, Version 2*, QuantumWise, Copenhagen, Denmark, 2017.
[33] J. P. Perdew, K. Burke, and M. Ernzerhof, "Generalized gradient approximation made simple," *Phys. Rev. Lett.*, vol. 77, no. 18, pp. 3865–3868, Oct. 1996.
[34] S. Grimme, "Semiempirical GGA-type density functional constructed with a long-range dispersion correction," *J. Comput. Chem.*, vol. 27, no. 15, pp. 1787–1799, Nov. 2006.
[35] X. Liang *et al.*, "Toward clean and crackless transfer of graphene," *ACS Nano*, vol. 5, no. 11, pp. 9144–9153, 2011.
[36] J. Kumar, A. Meersha, A. Gupta, and M. Shrivastava, "A first principle insight into defect assisted contact engineering at the metal-graphene and metal-phosphorene interfaces," in *Proc. Int. Conf. Simulation Semiconductor Processes Devices (SISPAD)*, Sep. 2019, pp. 1–4.
[37] F. Schwierz, "Graphene transistors," *Nature Nanotechnol.*, vol. 5, no. 7, pp. 487–496, 2010.